Electronic Supplementary Material (ESI) for Chemical Communications.

Supporting Information

Identification of pyrone-type species as the active site for oxygen reduction reaction

Zhao-Hong Sun,‡[a] Xue Zhang,‡[b] Xiao-Dong Yang,*[a] Wen-Na Shi,[a] Yan-Qing Huang,[a] Yong-Ling Men,[a] Jing Yang,[c] and Zhi-You Zhou*[c]

a College of Materials Science and Engineering, Xiamen Key Laboratory of Optoelectronic Materials and Advanced Manufacturing, Huaqiao University, Xiamen, Fujian 362021, People's Republic of China

b Institute of Advanced Materials Science and Engineering, Shenzhen Institutes of Advanced Technology, Chinese Academy of Sciences, Shenzhen 518055, China

c Collaborative Innovation Center of Chemistry for Energy Materials, State Key Laboratory of Physical Chemistry of Solid Surfaces, Tan Kah Kee Innovation Laboratory, College of Chemistry and Chemical Engineering, Xiamen University, Xiamen, Fujian 361005, People's Republic of China.

‡ These authors contributed equally to this work.

Corresponding author: xdyang@hqu.edu.cn (Xiao-Dong Yang), zhouzy@xmu.edu.cn (Zhi-You Zhou)

Table of contents

1. Experimental section
    1.1 Preparation of catalysts
    1.2 Electrochemical measurements
    1.3 Physical Characterization
    1.4 Boehm titration
    1.5 DFT calculations
2. Comparison between N-1000 and NAr-1100 catalysts
3. Characterization of oxygen-doped carbon-based catalysts
4. Proposed structure of intermedia during ORR
5. References

1. Experimental Section

1.1 Preparation of Catalysts

Ar-600 catalyst was prepared from carbon black (Ketjenblack EC-600JD from AkzoNobel). An acid-leaching step was firstly applied by dispersing 2 g of carbon black in 5 mol·L^{-1} hydrochloric acid solution at 80 ^{o}C for 12 h, followed by centrifugation, washing with deionized water, and drying at 80 ^{o}C for 12 h. The obtained powder was subsequently treated by an alkaline etching. In detail, they were dispersed in 100 mL KOH solution (2 mol·L^{-1}), then centrifuged and dried at 80 ^{o}C for 12 h. Finally, the KOH-contented carbon powder was heated at 600 ^{o}C for 2 h in an argon atmosphere. The final powder was named Ar-600 catalyst.

Ar-1100 catalyst was prepared by heating Ar-600 catalyst again at 1100 ^{o}C for one hour in an argon atmosphere.

N-1000 catalyst was prepared by heating Ar-600 catalyst at 1000 ^{o}C for one hour in ammonia (10 *wt.*% in argon) atmosphere.

NAr catalysts were processed with a second heat treatment for the N-1000 catalyst in an argon atmosphere at high temperatures, e.g., 1100 ^{o}C, 1200 ^{o}C, 1300 ^{o}C and 1400 ^{o}C, respectively. They were named NAr-1000, NAr-1200, NAr-1300 and NAr1400, respectively.

1.2 Electrochemical measurements

Electrochemical measurements were performed using a CHI-760D bipotentiostat equipped with a three-electrode system. A Pt ring/glassy carbon disk electrode (RRDE, Cat. No. 012613, BAS Inc.) coated with catalysts film was used working electrode. The ring size was 5 mm in inner diameter and 7 mm in outer diameter. The disk size was 4 mm in diameter. The collection coefficient was 37 % as calibrated by $Fe(CN)_6^{3+}$ /$Fe(CN)_6^{2+}$ redox as shown in Figure S1. A graphite plate was used as the counter electrode. A saturated calomel electrode (SCE) was used as a reference electrode. A locker, that allows ion connection while limiting ion diffusion, was designed between the reference electrode and main chamber to prevent chlorine ion contamination

from the reference electrode.

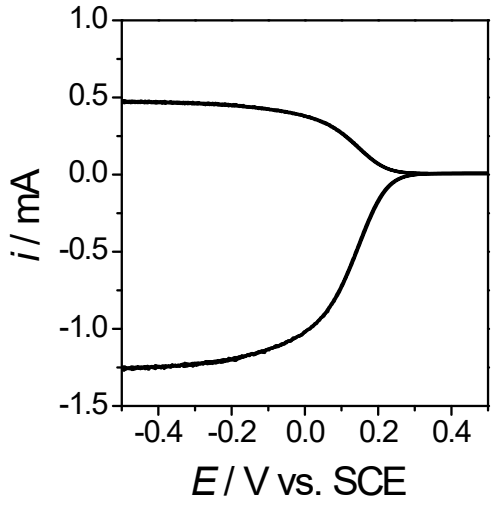

Figure S1. Calibration of collection efficiency by $Fe(CN)_6^{3+}$ /$Fe(CN)_6^{2+}$ redox in 5 mmol·L^{-1} $K_3Fe(CN)_6$+0.1 mol·L^{-1} KCl. E_{disk} is scaning between 0.5~-0.5 V *vs.* SCE, and E_{ring} is 0.28 V *vs.* SCE.

The catalyst ink was prepared by dispersing Fe/N/C catalyst powder (6.0 mg) in deionized water (300 μL), ethanol (650 μL) and Nafion solution (5 *wt.*% in n-propyl alcohol solution, 50μL). The catalyst ink was pipetted onto the glassy carbon disk and dried to form a catalyst film.

1.3 Physical Characterization

X-ray photoelectron spectroscopy (XPS) was employed to detect the surface element composition on Thermo ESCALAB 250Xi with 1486.71 eV Al Ka radiation. XPS spectra were referenced to the carbon C 1s peak at 284.6 eV. The N 1s spectra were deconvoluted into pyridinic-type N (398.8 eV), metal-N (399.9 eV), and graphitic-type N (401.2 eV).[1] The O 1s spectra were deconvoluted into highly conjugated forms of carbonyl oxygen such as quinine (Ph=O, 530.7 eV), carbon-oxygen double bond (-C=O, 531.4 eV), carbon-oxygen ether-like single bond (C-O-C, 532.4 eV) and carbon-oxygen single-bonds in hydroxyl groups (C-OH, 533.7 eV).[2] The fitted curves were represented by 80% Gaussian/ 20% Lorentzian line shape after Shirley-type background subtraction. The full width at half-maximum for each type of nitrogen component used for fitting was limited to the range of 1.1~1.50 eV.

The argon adsorption-desorption isotherms of the catalysts were tested on ASAP 2020 analyzer (Micromeritics). The specific surface area was determined through Brunauer-Emmett-Teller (BET) method.

Transmission electron microscopy (TEM, 200 kV, JEM-2100) was used to study the morphology and structure of catalysts.

Fourier transform infrared spectrophotometer (FT-IR, Thermo Scientific, NICOLET iS5) was used to detect the functional groups on the surface of catalysts.

Oxygen/Nitrogen Element Analyzer (Japan HORIBA, EMGA-620W) was used to test the content of oxygen and nitrogen in materials, and the average of three measurements on the sample.

1.4 Boehm titration

Boehm titration was used in this work to study the oxygen functional groups in the carbon surface. Here, experimental details of Boehm titration were described. The as-prepared catalysts were divided into several aliquots of 20 mg. Meanwhile, the initial solutions (before the addition of catalyst) were diluted solutions of either H_2SO_4 or NaOH at pH range of 1~11. The initial pH of solution was stabilized and measured after complete expulsion of CO_2 by pump-purge cycles with argon gas. The 20 mg of catalyst was added to 10 mL of the initial solution. After neutralization of surface groups and solution at 4 h, the final pH of solution was measured. The obtained initial and final pH was plotted as shown in Figure 2a and Figure S8. Modeling of fitting curves was described in Frédéric Jaouen's work, which showed how to extract the value of pK_a and basic site density[3]. Briefly, the inflection point at pH<5 was used to calculate the site density of basic groups, B_0, by the equation of $pH_{initial,\ inflection}$=-log$B_0$. And the final pH of plateau was equaled to 7 + 0.5 log(B_0) + 0.5 pK_a. Thus, the pK_a of the most frequently occurring basic groups was obtained.

1.5 DFT calculations

Density functional theory (DFT) calculations were carried out by using the CP2K code.[4] The basis set is a mixed Gaussian plane wave and the Perdew-Burke-Ernzerhof (PBE) generalized gradient approximation exchange-

correlation functional[5] was used to calculate the exchange-correlation energy. The DZVP-MOLOPT basis set in combination with Geodecker-Teter-Hutter pseudopotentials[6] was used with a plane wave cutoff energy of 450 eV. The structural minimization was performed using a Broyden–Fletcher–Goldfarb–Shanno algorithm[7]. Spin-polarized (local-spin-density approximation) and spin-unpolarized calculations (local-density approximation) were performed in the cases of odd and even numbers of electrons, respectively.

2 Comparison between N-1000 and NAr-1100 catalysts

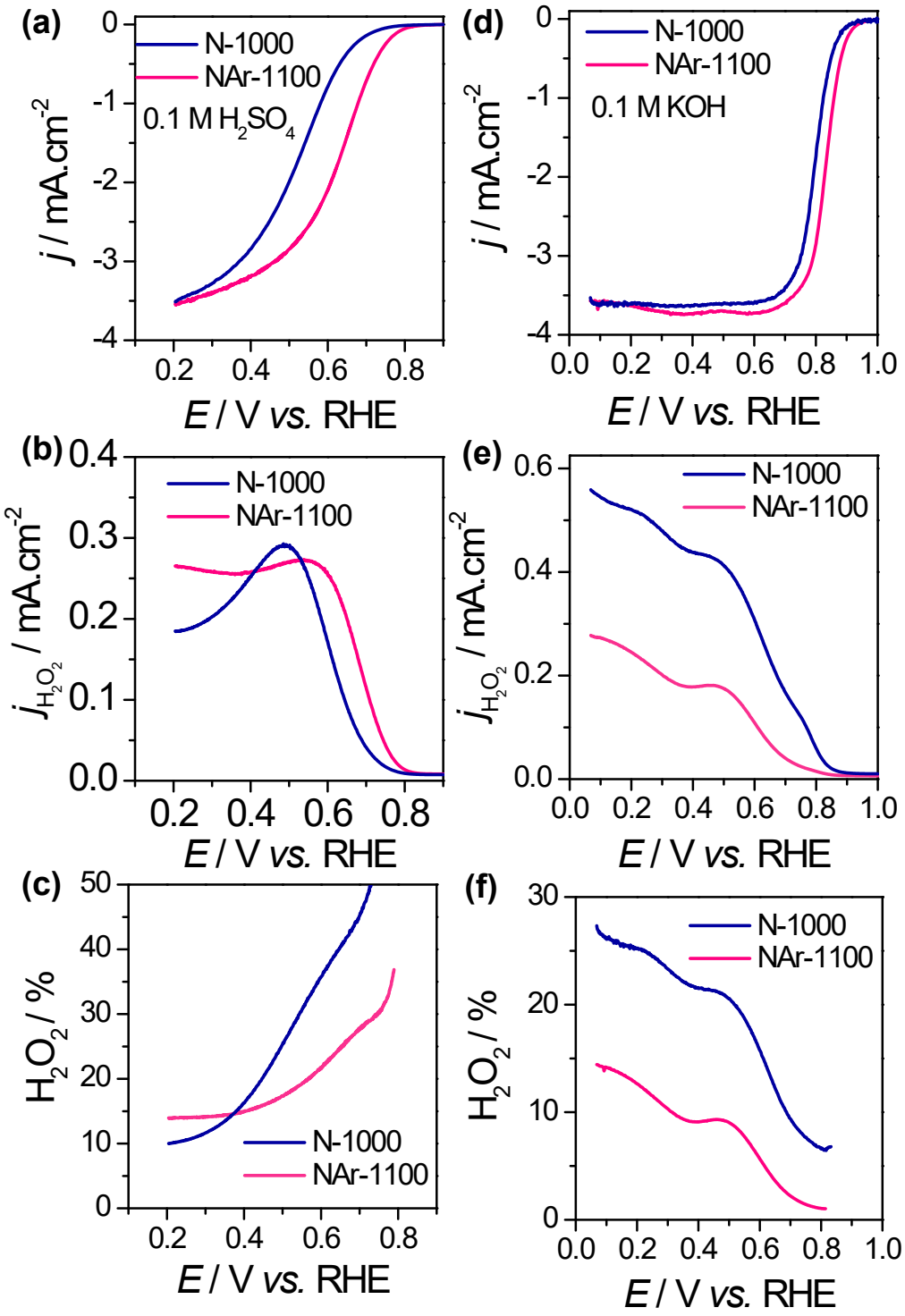

Figure S2. ORR activity of N-1000 and NAr-1100 catalysts in 0.1 mol·L^{-1} H_2SO_4 solution (**a~c**) and 0.1 mol·L^{-1} KOH solution (**d~f**) with O_2-saturated. The ORR current densities of catalysts were normalized to the geometric area (**a**) and (**d**). The current density of ORR converted to H_2O_2, determined by the platinum ring

was normalized to the geometric area of disc (**b**) and (**e**). The selectivity of H_2O_2 was calculated by the 37 % of collection coefficient (**c**) and (**f**).

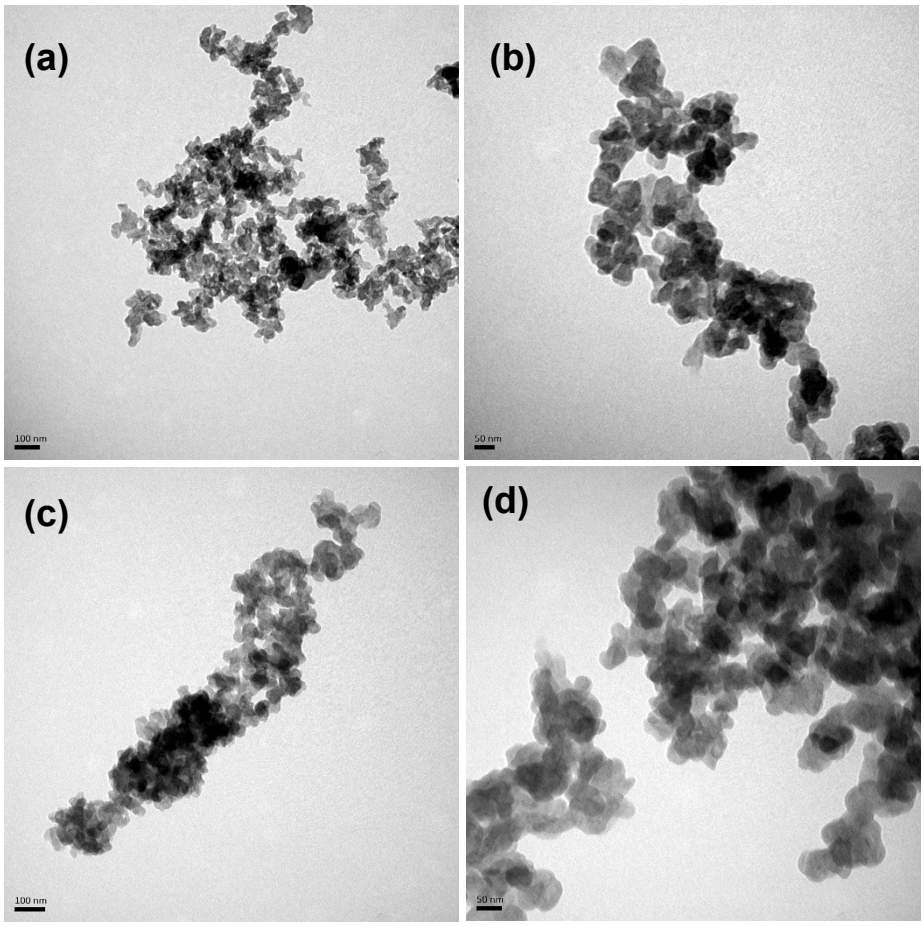

Figure S3. TEM image of N-1000 (**a-b**) and NAr-1100 (**c-d**) catalysts. The scale bar is 100 nm in (**a**) and (**c**), 50 nm in (**b**) and (**d**). Similar particle size and morphology were observed.

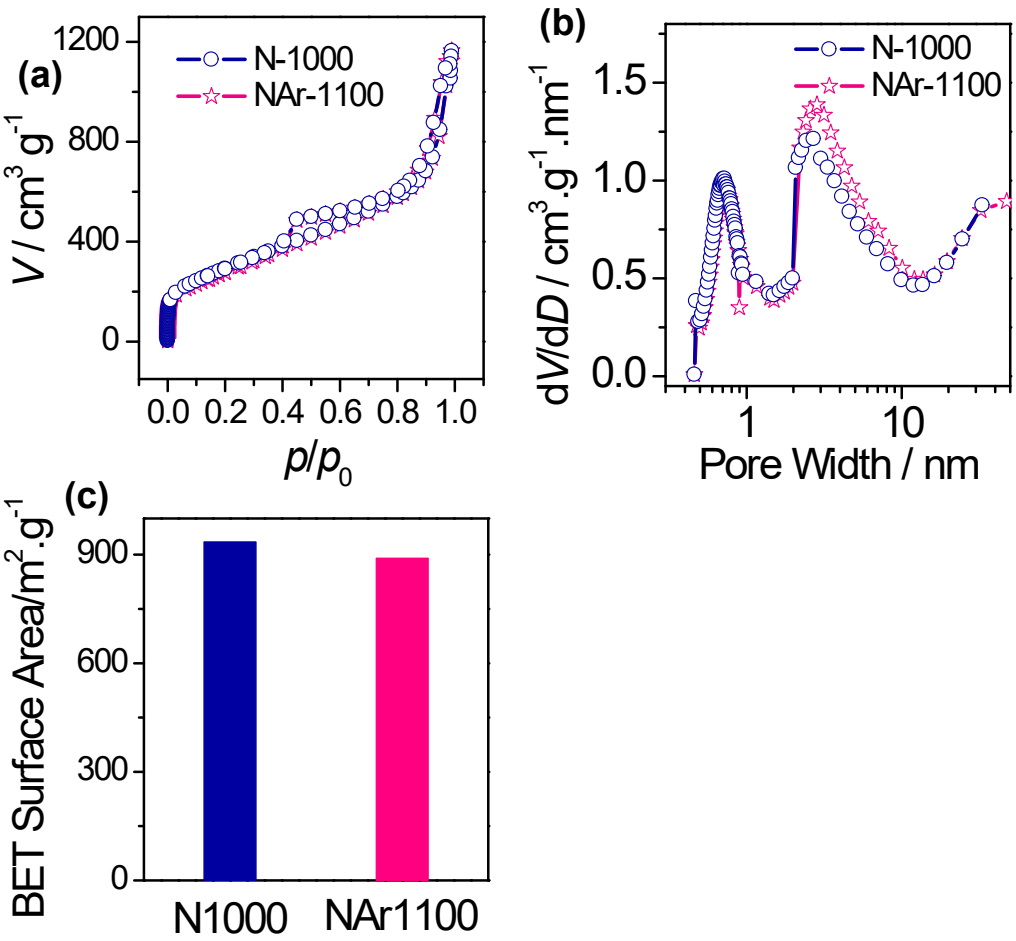

Figure S4. (**a**) Argon adsorption and desorption isotherms, (**b**) pore distribution and (**c**) the BET area of N-1000 and NAr-1100 catalysts. The same properties were observed again. It indicated the difference in ORR activity between N-1000 and NAr-1100 catalysts could not be derived from specific surface areas.

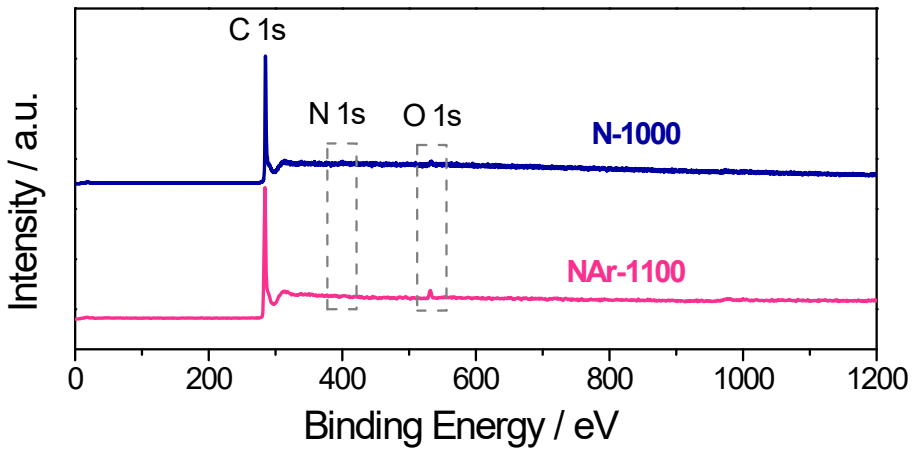

Figure S5. The XPS spectra of survey for N-1000 and NAr-1100 catalysts.

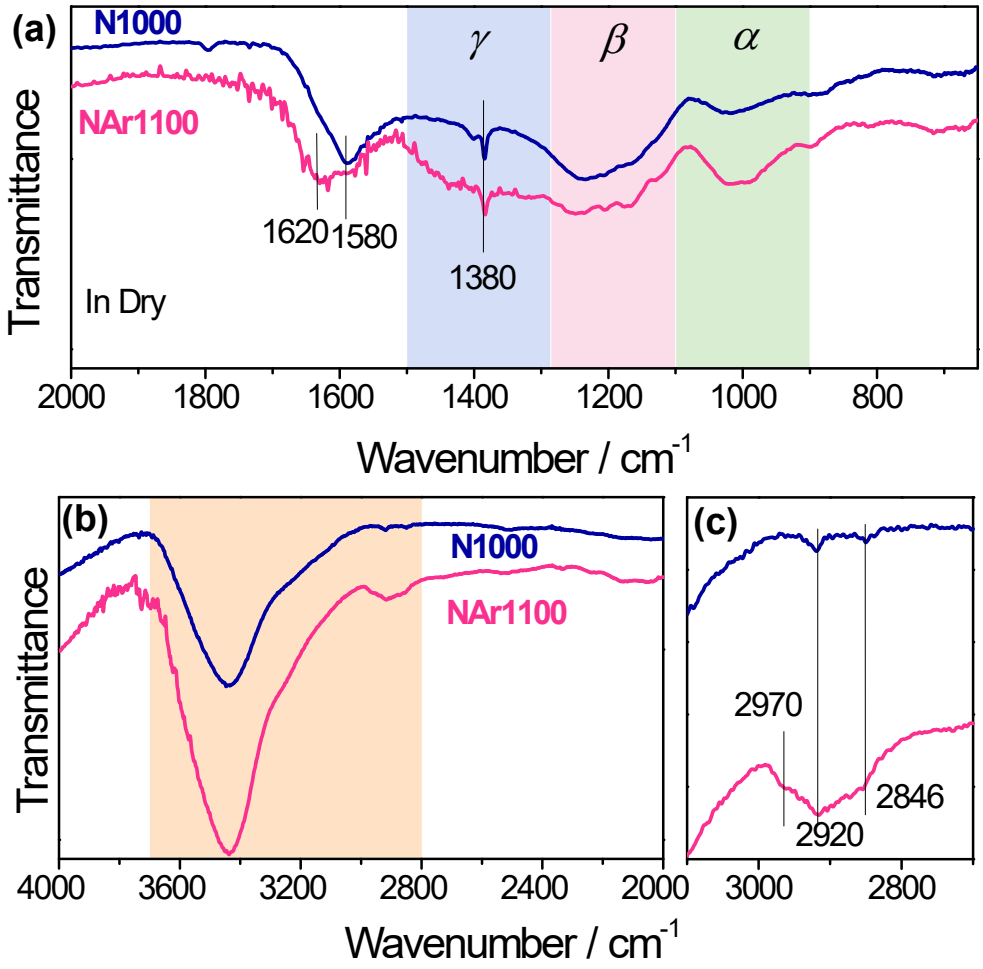

Figure S6. Transmission IR spectra of N-1000 and NAr-1100 catalysts. Wavenumber of 650 cm^{-1} to 2000 cm^{-1} shown in (**a**), Wavenumber of 2000 cm^{-1} to 4000 cm^{-1} shown in (**b**), and wavenumber of 2700 cm^{-1} to 3100 cm^{-1} enlarged in (**c**).

As shown in Figure S6a, the regions of spectral overlap (850~1500 cm^{-1}) involving mostly C–O and C=O contributions are divided into three regions: the *α*-region (900^{-1}~1100 cm^{-1}), *β*-region (1100^{-1}~1280 cm^{-1}) and *γ*-region (1280^{-1}~1500 cm^{-1}). According to the previous DFT calculations of carbon clusters, the ethers dominate in the *α* region with weaker contributions from hydroxyl and carboxyl, whereas weak absorptions of carbonyl (mainly pyrones and *γ*-butyrolactones) are more likely to fall in the *β* region. Both groups in *α* region and *β* region also have modes in the *γ* region, as well as the epoxides.[8, 9]

The most difference between N-1000 and NAr-1100 catalysts in Figure S6a was the peak at 1620 cm^{-1}. NAr-1100 catalyst has a peak at 1620 cm^{-1},

while it is none in N-1000 catalyst. There is a confusing assignment of 1620 cm^{-1}. The scissor mode of physically absorbed water, ketone and aromatic carbon double bounds all occur at 1620 cm^{-1}.[10-12] The C=C band, nearby conjugated carbonyl groups (e.g., pyrone), shifts to 1650−1600 cm^{-1} as a result of conjugation.[11] If the 1620 cm^{-1} peak is assigned to the absorbed water, it means the water content in the NAr-1100 is higher than that in N-1000 catalyst. Since the water is absorbed by the hydrogen bond between water and basic groups (carbonyl and ether groups), it also evidences more basic groups in NAr-1100 than that in N-1000 catalyst. Therefore, the peak at 1620 cm^{-1} in NAr-1100 catalyst confirmed that it has more carbonyl and ether groups than N-1000 catalyst, no matter whether the 1620 cm^{-1} peak is assigned to absorbed water or the C=C band nearby conjugated carbonyl groups.

Another difference was the peak at 2846 cm^{-1}, 2920 cm^{-1}, and 2970 cm^{-1} as shown in Figure S6c. The three peaks are observed in NAr-1100 catalyst. They are ascribable to the *u*(C−H) vibration of the $-CH_2-$ group in *ortho*-benzopyran and *para*-benzopyran.[11] It means there are some ether groups in NAr-1100 catalyst.

To sum up, the NAr-1100 catalyst has more carbonyl and ether groups than the N-1000 catalyst.

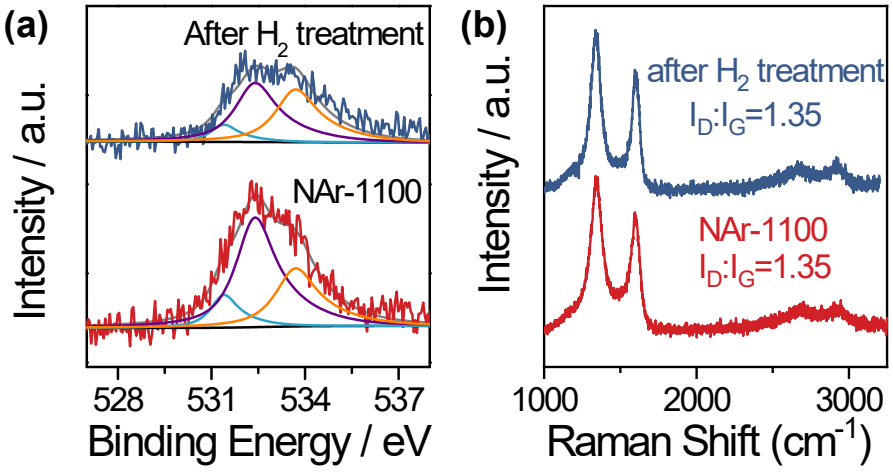

Figure S7. Comparison of NAr-1100 before and after heat treatment in hydrogen gas at 1100 °C. (**a**) High-resolution O 1s spectra. (**b**) Raman spectra.

To prove the role of the oxygen-containing functional group in ORR, the NAr-1100 catalyst was further treated with hydrogen gas at 1100 °C. It is supposed to only remove the functional groups but retain defect sites (e.g. pentagon rings) in such a reduction condition since the graphitization temperature is up to 2900 °C. This is evidenced by the decreased oxygen content (Figure S7a) and the unchanged defect density (Figure S7b) after treatment in hydrogen gas. Meanwhile, the ORR activity is highly decreased in acid electrolytes after hydrogen treatment (Figure 1d). It means the main active sites have been removed by the hydrogen heat treatment and these sites are the oxygen-containing functional groups.

3. Characterization of oxygen-doped carbon-based catalysts

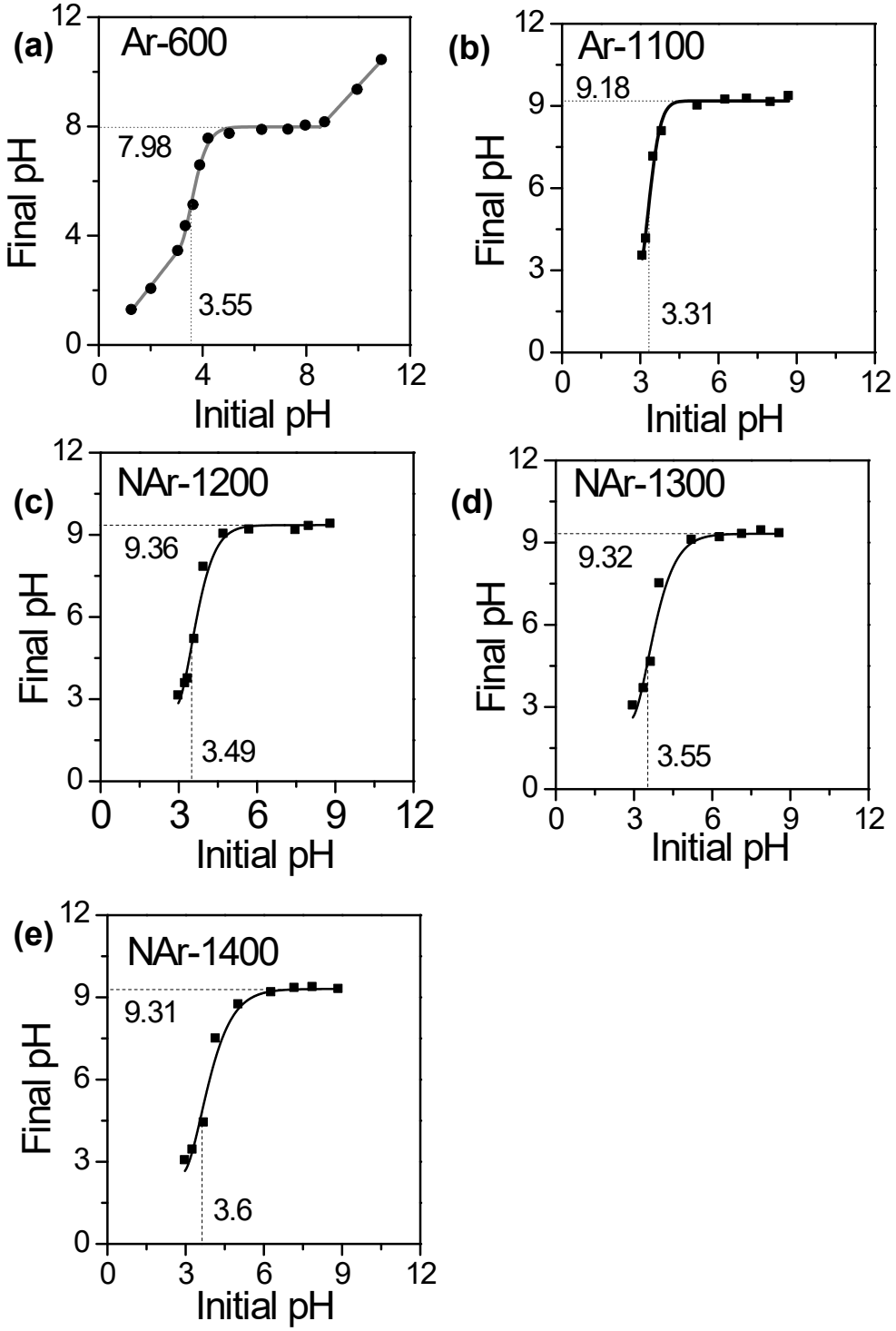

Figure S8. Boehm titration curves of Ar-600 (**a**), Ar-1100 (**b**), NAr-1200 (**c**), NAr-1300 (**d**) and NAr1400 (**e**).

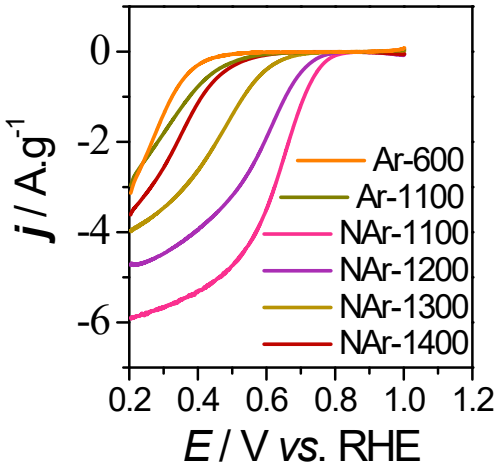

Figure S9. Mass ORR activity of a series of carbon-based catalysts with oxygen-doped, including Ar-1100, NAr-1100, NAr-1200, NAr1300 and NAr-1400 catalysts in oxygen-saturated 0.1 mol·L^{-1} H_2SO_4 solution.

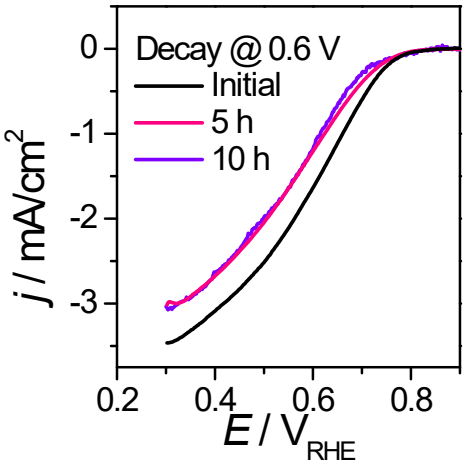

Figure S10. Ten-hour stability of NAr-1100 at 0.6 V *vs.* RHE in oxygen-saturated 0.1 mol·L^{-1} H_2SO_4 solution.

Table S1. Oxygen/Nitrogen Elemental Analysis

	Oxygen / at.%	Nitrogen / at.%
NAr-1100	1.85±0.04	0.40±0.07
NAr-1200	1.81±0.04	0.22±0.05
NAr-1300	1.45±0.08	0.19±0.04
NAr-1400	1.35±0.03	0.19±0.02

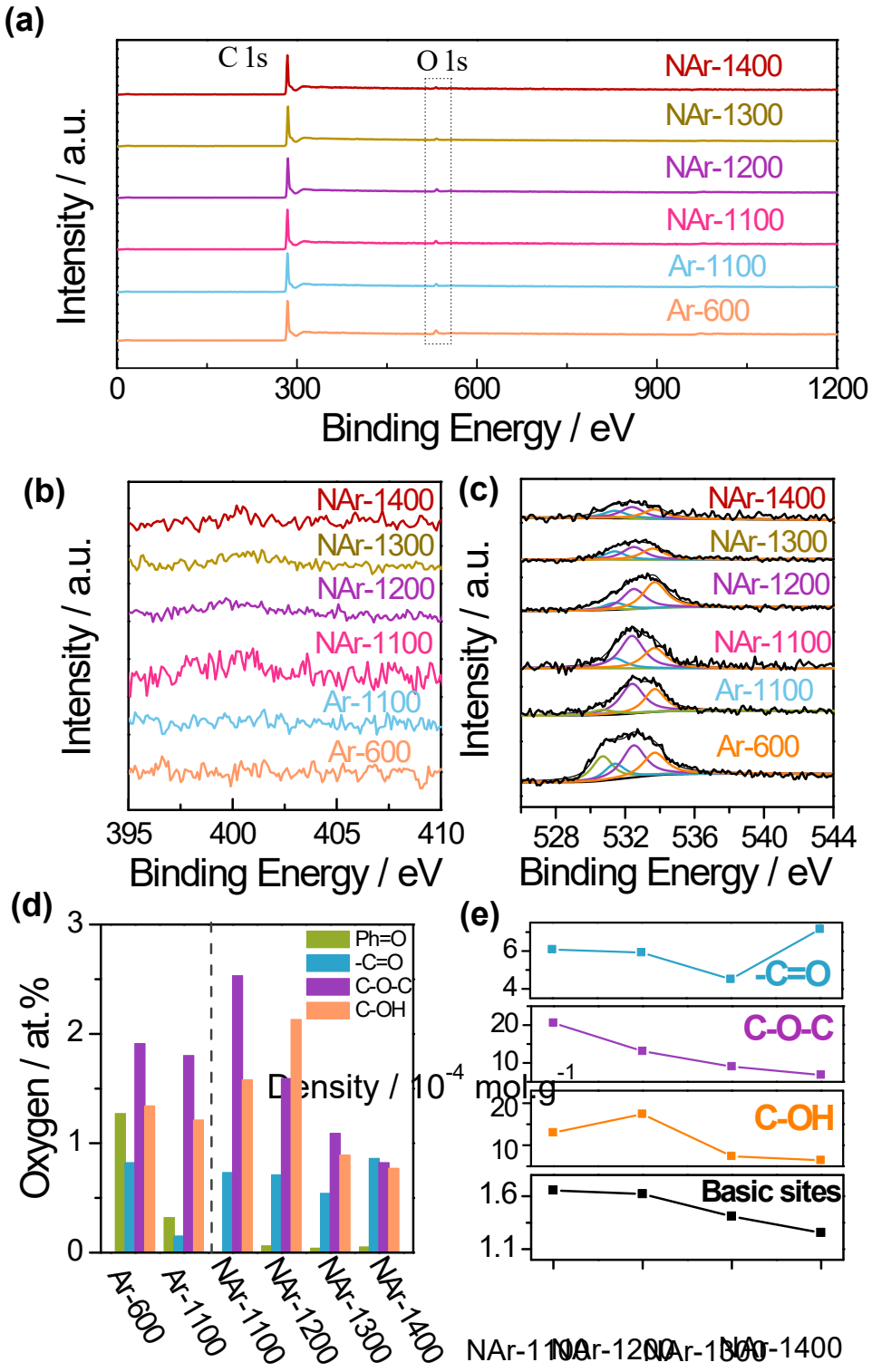

Figure S11. The XPS spectra of survey (**a**), high-resolution XPS of N 1s (**b**), high resolution of O 1s (**c**) and oxygen content (**d**) for O-carbon catalysts, included for Ar-600, Ar-1100, NAr-1100, NAr-1200, NAr1300 and NAr-1400 catalysts. (**e**) Site density of oxygen-contented functional groups. From top

column to bottom column were the site density of carbonyl oxygen (sp^2), etheric oxygen (sp^3), hydroxyl oxygen and basic groups, respectively.

As shown in table S1, Figure S11a and S11b, the nitrogen has almost burned out in the two-steps heat treatment catalysts (NAr-1100 to NAr-1400). Oxygen was the only considerable doped element in these catalysts (Figure S11a). The oxygen spectra (Figure S11c) were deconvoluted into highly conjugated forms of carbonyl oxygen such as quinine (Ph=O, 530.7 eV), carbon-oxygen double bond (-C=O, 531.4 eV), carbon-oxygen ether-like single bond (C-O-C, 532.4 eV) and carbon-oxygen single-bonds in hydroxyl groups (C-OH, 533.7 eV). The oxygen atom ratio was calculated as shown in Figure S11d and converted to site density as shown in Figure S11e. It is worth noting that the basic site density is much lower than the density of oxygen-containing functional groups. Here are two reasons. One is that the XPS is a near-surface analytical method. While the Boehm titration was a strict surface analytical method. Moreover, the basic site density counted by the Boehm titration was lower than the real one due to the accessibility of hydrogenated water to basic sites. Another reason is that basic sites do not directly correlate with oxygen functional groups, but correlate to the conjugated structures, such as pyrone-type species. Carbonyl oxygen exhibits Bronsted-basic property to bind with proton, when it is conjugated with etheric oxygens in the pyrone-type species. While the isolated etheric oxygens (chromene-type species, **1** in Figure 3a) are very weak bases (pK_a=-2~-4 of ethers)[13]. Such weak bases are outside the pH range of present titration (pH range of 3~9) and cannot be detected.

Furthermore, the basicity and redox activity of carbon surfaces should be discussed in a global view. As commented by previous report,[14] the basicity and redox activity are mainly determined by the global distribution of peripheral etheric and carbonyl rings rather than specific functional groups. It means the direct correlation between ORR activity and the amount of specific functional groups may conduct to a wrong conclusion. This is because these functional groups are highly conjugate and easily affected by each other. For example, the carbonyl oxygens in the quinone-type species (Ar-600) and the pyrone-type species (NAr-1100) exhibit different pK_a (5.5 *vs.* 8.2 as shown in Figure 2c) and ORR activity (Figure 2b and Figure 3c). While in the Boehm titration, the

obtained pK_a reflects the local structure by considering the conjugate property of functional groups and carbon matrix. Benefiting from the similar working environment of the Boehm titration and electrochemical test, the structure of catalysts could be measured in a real working state and is supposed to be accurate in the study of the structure-activity relationship.

4. Proposed structure of intermedia during ORR

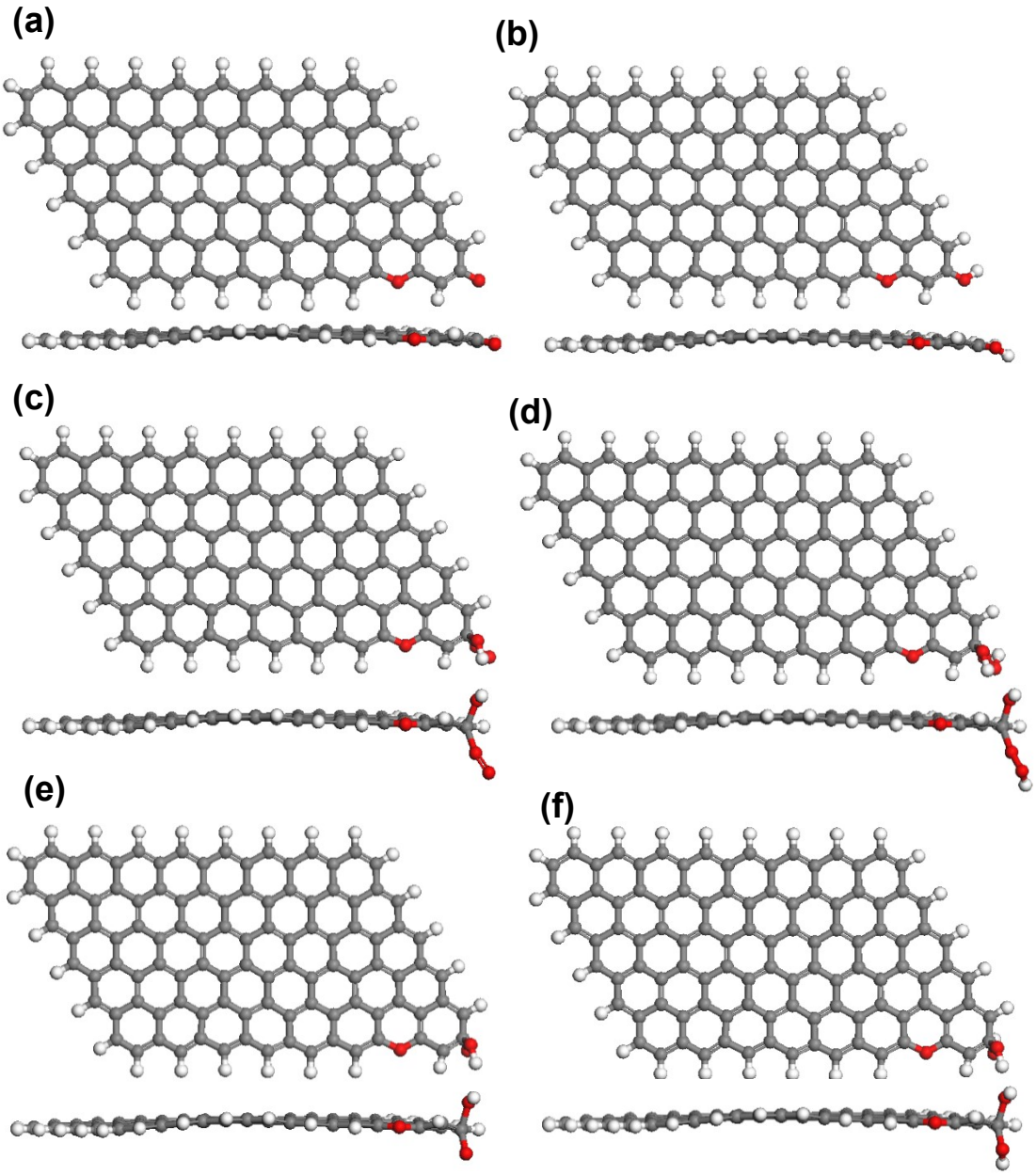

Figure S12. The optimized configurations as shown in Figure 4 used for the free energy calculations. (**a**) bicyclic pyrone-type species (**4**), (**b**) hydrogenated bicyclic pyrone-type species (**6**), and (**c-f**) ORR intermediates on the bicyclic pyrone-type species.

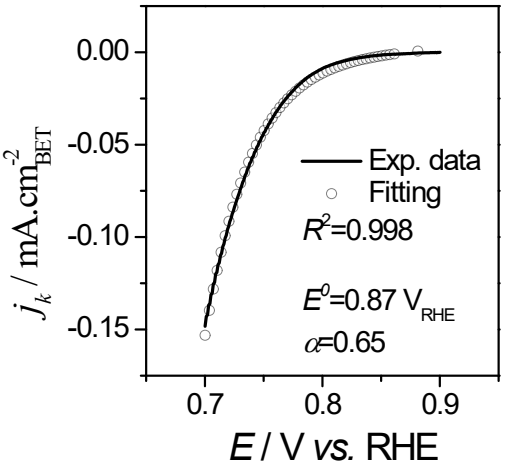

Figure S13. The polarization curve of NAr-1100 catalyst in acid solution was fitted by the Butler-Volmer equation.

$$j = j^0(e^{-\alpha f(E-E^0)} - e^{(1-\alpha)f(E-E^0)})$$

Here, j is the kinetic current density, j^0 is the exchange current density, α is the electron transfer coefficient, E is the applied potential, and E^0 is the equilibrium potential of the rate-determining step (RDS). According to the DFT calculations as shown in Figure 4a, the first electron transfer during ORR (**7**→**8**) is the RDS. The fitting E^0 from the experimental data (0.87 V_{RHE} in Figure S13) is agreed with that from the DFT calculation (0.86 V=1.23 - 0.37 V).

5 References

1. X.-D. Yang, Y. Zheng, J. Yang, W. Shi, J.-H. Zhong, C. Zhang, X. Zhang, Y.-H. Hong, X.-X. Peng, Z.-Y. Zhou and S.-G. Sun, *ACS Catal.*, 2017, **7**, 139-145.
2. R. Arrigo, M. Hävecker, S. Wrabetz, R. Blume, M. Lerch, J. McGregor, E. P. J. Parrott, J. A. Zeitler, L. F. Gladden, A. Knop-Gericke, R. Schlögl and D. S. Su, *J. Am. Chem. Soc.*, 2010, **132**, 9616-9630.
3. J. Herranz, F. Jaouen, M. Lefèvre, U. I. Kramm, E. Proietti, J.-P. Dodelet, P. Bogdanoff, S. Fiechter, I. Abs-Wurmbach, P. Bertrand, T. M. Arruda and S. Mukerjee, *J. Phys. Chem. C*, 2011, **115**, 16087-16097.
4. J. VandeVondele, M. Krack, F. Mohamed, M. Parrinello, T. Chassaing and J. Hutter, *Comput. Phys. Commun.*, 2005, **167**, 103-128.
5. J. P. Perdew, K. Burke and M. Ernzerhof, *Phys. Rev. Lett.*, 1996, **77**, 3865-3868.
6. S. Goedecker, M. Teter and J. Hutter, *Phys. Rev. B*, 1996, **54**, 1703-1710.
7. W. H. Press, S. A. Teukolsky, W. T. Vetterling and B. P. Flannery, *Numerical Recipes: The Art of Scientific Computing*, Cambridge University Press, 3rd edn., 2007.
8. M. Acik, G. Lee, C. Mattevi, A. Pirkle, R. M. Wallace, M. Chhowalla, K. Cho and Y. Chabal, *J. Phys. Chem. C*, 2011, **115**, 19761-19781.
9. A. Bagri, C. Mattevi, M. Acik, Y. J. Chabal, M. Chhowalla and V. B. Shenoy, *Nat. Chem.*, 2010, **2**, 581-587.
10. E. Fuente, J. A. Menéndez, M. A. Díez, D. Suárez and M. A. Montes-Morán, *J. Phys. Chem. B*, 2003, **107**, 6350-6359.
11. A. Barroso-Bogeat, M. Alexandre-Franco, C. Fernández-González and V. Gómez-Serrano, *Energy & Fuels*, 2014, **28**, 4096-4103.
12. C. Zhang, D. M. Dabbs, L.-M. Liu, I. A. Aksay, R. Car and A. Selloni, *J. Phys. Chem. C*, 2015, **119**, 18167-18176.
13. D. D. Perrin, B. Dempsey and E. P. Serjeant, *pKa Prediction for Organic Acids and Bases* Springer, Dordrecht, 1 edn., 1981.
14. E. Fuente, J. A. Menéndez, D. Suárez and M. A. Montes-Morán, *Langmuir*, 2003, **19**, 3505-3511.